CRYSTAL PLASTICITY ANALYSIS OF DISLOCATION EMISSION FROM MICRO VOIDS

Tetsuya Ohashi *

Kitami Institute of Technology, Koencho 165, Kitami, Hokkaido, Japan

Abstract:

Slip deformation in the vicinity of a micro void in metal crystals is analyzed by a crystal plasticity technique, and the geometrically necessary dislocations, which accompany the gradient of plastic shear strain on slip systems, are evaluated. Aggregates of dislocation segments on pairs of slip systems that have the same slip directions but different slip planes exhibit a rhombus-shaped structure, and the structure is shown to be equivalent to prismatic dislocation loops of the interstitial type. Material transport and growth of voids are discussed in terms of GN dislocations.

Keywords: A, dislocations; A, microstructures; A, voids and inclusions; B, crystal plasticity.

* e-mail ohashi@newton.mech.kitami-it.ac.jp, tel./fax. +81-157-26-9227

1. Introduction

Growth of micro voids and material transport during the process of plastic deformation in microstructures of metal crystals play important roles in the nonlinear deformation and fracture processes. There have been many studies on void growth and some studies were added recently on the effect of mutual interaction between multiple voids (for example, Orsini and Zikry, 2001; Schacht, *et al*., 2003; and Tvergaard and Niordson, 2004) and on voids near hetero-interfaces (Li and Guo, 2002; Li *et al*., 2003; Siruguet and Leblond, 2004; Bonfoh *et al*., 2004) or at a crack tip (Baaser and Gross, 2003). Much interest has been shown in the mechanism of void growth and its quantitative evaluation from atomistic and crystallographic viewpoints. Localized slip deformation near a void surface due to stress concentration and dislocation emission (for example, Lubarda *et al*., 2004) seem to be essential processes for material transport and growth of the voids.

A series of atomistic simulation studies on emission of prismatic dislocation loops has been carried out by Rudd and Belak (2002), Rudd (2002), Belak (1998a, 1998b), Belak and Minich (1999) and Moriarty *et al*. (2002). In those studies, a molecular dynamics cell with a spherical-shaped void was subjected to external shock loading, and defect structures of partial dislocations and prismatic dislocation loops of interstitial type were observed. On the other hand, we recently examined plastic slip deformation near a secondary particle by crystal plasticity finite element analysis (Ohashi, 2002; Ohashi and Asakawa, 2002; Ohashi, 2004a). When the particle underwent a dilatational phase transformation, we observed the three-dimensional structure of the

geometrically necessary (GN) dislocations. The entire structure of the dislocations was a diamond shape and they corresponded to prismatic dislocation loops of the interstitial type.

In this paper, slip deformation in a model of a single crystal with a spherical-shaped void region that is subjected to tri-axial tensile loading is examined by the crystal plasticity finite element technique. Spatial distribution of the GN dislocation segments and their characteristics are examined in a quantitative manner. Aggregates of GN dislocation segments are shown to make structures of prismatic dislocation loops around the void. The amount of material transport near the void is estimated in terms of GN dislocations.

2. Crystal plasticity analysis and evaluation of statistically stored and geometrically necessary dislocations

Let us consider slip deformation in face centered cubic type crystals where slip takes place on the {111} crystal planes and in the <110> crystal directions. The combinations of these slip planes and slip directions define twelve slip systems as shown in Table 1. The activation condition of the slip system *n* is given by the Schmid law:

$$P_{ij}^{(n)}\sigma_{ij} = \theta^{(n)}, \quad P_{ij}^{(n)}\dot{\sigma}_{ij} = \dot{\theta}^{(n)}, \quad (n = 1,\cdots,12), \tag{1}$$

and

$$P_{ij}^{(n)} = \frac{1}{2}\left(\nu_i^{(n)}b_j^{(n)} + \nu_j^{(n)}b_i^{(n)}\right), \tag{2}$$

where σ_{ij} and $\theta^{(n)}$ denote the stress and the critical resolved shear stress on slip system *n*, respectively. The Schmid tensor $P_{ij}^{(n)}$ is defined by the slip plane normal $\nu_i^{(n)}$ and the slip direction $b_i^{(n)}$. Quantities with dots indicate incremental quantities. An increment of the critical resolved shear stress is written as follows:

$$\dot{\theta}^{(n)} = \sum_m h^{(nm)}\dot{\gamma}^{(m)}, \tag{3}$$

where $\dot{\gamma}^{(m)}$ denotes the increment of plastic shear strain on slip system *m*. If the deformation is small and rotation of the crystal orientation is neglected, the constitutive equation for slip deformation is written as follows (Hill, 1966; Ohashi, 1987):

$$\dot{\varepsilon}_{ij} = [S^{e}_{ijkl} + \sum_{n}\sum_{m}\{h^{(nm)}\}^{-1}P^{(n)}_{ij}P^{(m)}_{kl}]\dot{\sigma}_{kl}\,. \tag{4}$$

S^{e}_{ijkl} denotes the elastic compliance, and the summation is made over the active slip systems.

We assume that the critical resolved shear stress is a function of the Bailey-Hirsch type and is given by the following equation (Ohashi, 1987, 1994):

$$\theta^{(n)} = \theta_0 + \sum_{m}\Omega^{(nm)}a\mu\tilde{b}\sqrt{\rho_S^{(m)}}\,, \tag{5}$$

where θ_0 and $\rho_S^{(m)}$ denote the lattice friction term, which is temperature-dependent in general, and the density of the statistically stored dislocations (abbreviated hereafter as SS dislocations) that accumulate on slip system *m*, respectively. In this paper, it is assumed that dislocation sources exist everywhere in the specimen and that slip deformation occurs where resolved shear stress reaches the critical value. The temperature is assumed to be a constant and thus, θ_0 is also a constant.

SS dislocations that have accumulated on the *m*-th slip system contribute

to the critical resolved shear stress of the *n*-th system through the component $\Omega^{(nm)}$. There are 12 x 12 components in $\Omega^{(nm)}$ and their values are given by five independent parameters, which are defined by elementary processes of interaction between dislocations on slip systems *n* and *m* (Ohashi, 1987, 1994). Table 2 shows the dislocation interaction and components of the interaction matrix, R1, R2, R3, R3' and R4. The relative magnitude of the off-diagonal to the diagonal components in the interaction matrix governs the latent hardening characteristics of slip systems. In the present paper, we choose the parameters $\mathrm{R1} \approx \mathrm{R2} \approx \mathrm{R3} \approx \mathrm{R3}' \approx \mathrm{R4} \approx 1$ to represent a nearly isotropic hardening character for every slip system. The elastic shear modulus μ and the magnitude of the Burgers vector $\tilde{b}$ are material constants and *a* is a numerical factor.

The increment in the density of the SS dislocations on the slip system *n* is given as follows (Ohashi, 1987, 1994):

$$\dot{\rho}_S^{(n)} = c\dot{\gamma}^{(n)} \Big/ \tilde{b}L^{(n)}, \tag{6}$$

where *c* is a numerical coefficient of the order of 1. $L^{(n)}$ denotes the mean free path of dislocations on slip system *n* and, in this paper, we use the following model for it (Ohashi, 2004b);

$$L^{(n)} = \frac{c^*}{\sqrt{\sum_m \omega^{(nm)} (s \cdot \rho_S^{(m)} + g \cdot \left\| \rho_G^{(m)} \right\|)}}, \tag{7}$$

where *c** is a material constant of the order of 10 - 100 (For detailed discussion,

see Kuhlmann-Wilsdorf, 1989.). $\left\|\rho_G^{(m)}\right\|$ denotes the density of the GN dislocations on slip system *m*. Weight matrix $\omega^{(nm)}$ is introduced here, and its components should be determined in a way similar to that for determination of components for $\Omega^{(nm)}$ from the viewpoint of dislocation interaction. Parameters *s* and *g* are introduced to control the analysis and $0 \le s \le 1$, $0 \le g \le 1$.

The edge and screw components of the GN dislocations are obtained from spatial gradients of the plastic shear strain on slip systems (Ohashi, 1997):

$$\rho_{G,edge}^{(n)} = -\frac{1}{\tilde{b}} \frac{\partial \gamma^{(n)}}{\partial \xi^{(n)}}, \qquad \rho_{G,screw}^{(n)} = \frac{1}{\tilde{b}} \frac{\partial \gamma^{(n)}}{\partial \zeta^{(n)}}. \tag{8}$$

Here, $\xi^{(n)}$ and $\zeta^{(n)}$ denote directions parallel and perpendicular to the slip direction on the slip plane, respectively. The norm of the two components gives the density of GN dislocations,

$$\left\|\rho_G^{(n)}\right\| = \sqrt{\left(\rho_{G,edge}^{(n)}\right)^2 + \left(\rho_{G,screw}^{(n)}\right)^2}. \tag{9}$$

The tangent vector $\mathbf{l}^{(n)}$ of the dislocation line segments is calculated as follows (Ohashi, 1999):

$$\mathbf{l}^{(n)} = \frac{1}{\left\|\rho_G^{(n)}\right\|}\left(\rho_{G,screw}^{(n)} \cdot \mathbf{b}^{(n)} + \rho_{G,edge}^{(n)} \cdot \mathbf{b}^{(n)} \times \mathbf{v}^{(n)}\right), \tag{10}$$

where $\mathbf{b}^{(n)}$ and $\mathbf{v}^{(n)}$ denote unit vectors parallel to the slip direction and slip

plane normal of the slip system *n*, respectively. Angle $\varphi^{(n)}$ between a dislocation line segment and the Burgers' vector defines the character of the segment (Figs. 1 and 2), which is obtained by the following equations.

$$\cos\varphi^{(n)} = \frac{\rho_{G,screw}^{(n)}}{\left\|\rho_G^{(n)}\right\|}, \qquad \sin\varphi^{(n)} = \frac{\rho_{G,edge}^{(n)}}{\left\|\rho_G^{(n)}\right\|}. \tag{11}$$

Positive and negative edge dislocation segments have the characteristic angles $\pi/2$ and $3\pi/2$, respectively, while positive and negative screw segments have the characteristic angles 0 and π (Fig. 2). A dislocation segment with the characteristic angle $\pi/3$, for example, is a mixture of edge and screw character and is usually called 60 degree mixed-type dislocation. Extra half plane of a dislocation segment with $0<\varphi^{(n)}<\pi$ exists on the side that $\mathbf{v}^{(n)}$ is pointing, and that of a dislocation segment with $\pi<\varphi^{(n)}<2\pi$ exists on the opposite side.

The strain hardening coefficient in equation (3) is given by the following equation:

$$h^{(nm)} = \frac{1}{2} ac\mu\,\Omega^{(nm)} / \left[L^{(m)} \sqrt{\rho_S^{(m)}} \right], \tag{12}$$

and by substituting eq. (7) into eq. (12), we have

$$h^{(nm)} = \frac{ac\mu}{2c^*}\,\Omega^{(nm)} \sqrt{\frac{\sum_k \omega^{(mk)} (s\cdot\rho_S^{(k)} + g\cdot\left\|\rho_G^{(k)}\right\|)}{\rho_S^{(m)}}}. \tag{13}$$

When $0 < g$, GN dislocations contribute to the strain hardening. Since the GN dislocation densities are scale-dependent quantities, the strain hardening characteristics are also scale-dependent (Ohashi, 2004b). For the purpose of introducing scale-dependent characteristics of materials, direct introduction of GN dislocations into the critical resolved shear stress has been discussed widely, but its relevance is still controversial (see, for example, Weertman, 2002). In this paper, we do not introduce GN dislocations into the expression of the critical resolved shear stress, but the scale-dependent characteristics appear through eqs. (7) and (13).

After finite element analysis, numerical data of GN dislocations are obtained for each element, and dislocation segments are graphically displayed in three-dimensional space. For the purpose of graphical representation, the length and thickness of each dislocation segment is determined as a function of dislocation density (Fig. 3), and their directions are determined by eq. (10). A color can also be assigned to each dislocation segment, assignment of color being determined as a function of the characteristic angle of the dislocation segment. In this paper, we assign green, blue-green, navy blue and red colors for dislocation segments with $\varphi =$ 0, $\pi/2$, π and $3\pi/2$, respectively. A dislocation segment with an intermediate value of characteristic angle is given a color between these colors. If we observe a clockwise loop of dislocation segments, within which plastic shear strain is larger than that outside the loop, its graphical representation should be like that given in Fig. 2.

3. Models for the analysis and numerical procedure

Fig. 4 shows the geometry of the model employed for numerical analysis. The lateral dimension of the entire model is 30 μm, and a spherical-shaped region, which represents the void, is positioned at the center of the model. The diameter of the void is 4 μm and its volume fraction is about 0.12%. The *x*, *y*, and *z* axes correspond to the three <100> crystal orientations.

Three surfaces of the model on $x=0$, $y=0$, and $z=0$ are not allowed to move in their normal directions, while uniform tensile displacement is applied on the remaining three surfaces. The average axial strain is defined by the applied tensile displacement divided by the specimen dimension of 30 μm. The average axial strains in the *x*, *y*, and *z* directions are always the same, since the applied displacements in these directions are the same. The average volumetric strain is obtained by the sum of the three average axial strains. Also, reaction forces are monitored at nodes on free surfaces, and average axial stresses (normal stresses in tensile directions) are calculated from them. The average axial stresses in *x*, *y*, and *z* directions are equal and positive. These stresses are hereafter called negative hydrostatic pressures since the word "pressure" is usually used for negative normal stresses.

Two models are used for determining characteristics of the matrix material. Model I has an idealized material characteristics: the elastic compliances are $S_{11}=1$, $S_{12}=-0.25$ and $S_{44}=2.5\times10^{-11}$ m^2/Pa, and the material is elastically isotropic. The magnitude of the Burgers vector $\tilde{b}$ is a typical value of 2.5×10^{-10} m. The lattice friction θ_0 is 10 MPa and parameter *a* in eq. (5) is given a sufficiently small value of 1×10^{-9}. Also, the parameter *c**

is given a large value of 100. With this combination of parameters, the second term in eq. (5), which causes the strain hardening of the slip systems, is negligibly small and the critical resolved shear stresses for slip systems will be kept constant at 10 MPa.

Material parameters for model II are chosen so that they represent a copper crystal. Table 3 shows the set of material parameters used for model II. Experimental data for Cu are used for the elastic compliances and $\tilde{b}$, and a typical value of 0.1 is given for a. Values for c^*, g, and s for dislocation mean free pass are chosen so that slip systems will harden by accumulations of GN and SS dislocations. Components of the weight matrix $\omega^{(nm)}$ are assumed to be 1 except when $n = m$ or slip systems n and m are co-planar. In the latter case of combinations of slip systems, $\omega^{(nm)} = 0$.

The model is divided into 7936+64 elements: 7936 elements are used for the matrix region, and 64 elements are used to model the void region, to which sufficiently large values are given for its elastic compliances. As a result, the void region deforms only elastically and bears no load. Within the matrix region, mesh size is finer near the void surface, especially in the direction perpendicular to it.

Finite element crystal plasticity analysis is performed by a software code *CLP* ver. 7 which we have developed. The element type used in this study is a composite element with eight nodes (Zienkiewicz, 1977). One composite element consists of five tetrahedral elements with linear shape functions. The deformation behavior is analyzed with the tetrahedral elements, while the data for dislocations are evaluated for each composite element with averaged data for stresses and strains in the tetrahedral elements. Nodal point data of the

plastic shear strain on twelve slip systems are evaluated by weighted average of the values in composite elements, which are connected to the node, and the strain gradients in elements are calculated from the nodal point data (Ohashi, 1997). For the time marching of the incremental analysis, we extend the algorithm proposed by Yamada *et al.* (1968). In this extended algorithm, small and varying increments of load sufficient to just cause activation of the successive slip systems or inactivation of an active system are applied. The constitutive relation of the element is revised in accordance with the new set of active slip systems and a new time step is then started.

4. Results and discussion

4.1 Prismatic dislocation loops in model I

Fig. 5(a) shows the GN dislocation segments obtained for the slip system B4 when the average volumetric strain is 0.053%. At this early stage of deformation, some groups of dislocation segments are observed to make up half-loop shaped structures. Fig. 5(b) and (c) show the GN dislocation segments obtained for the same slip system when the average volumetric strain is 0.199%. There are two pairs of groups of dislocation segments. One pair is in front of the void region, which can be seen in Fig. 5(b) and (c), and the other is behind the void region. Characteristic angles of the dislocation segments in one group in front of the void are close to $-\pi/3$, and the angles of the segments in the other group are close to $\pi/3$. The density of dislocations within these groups is calculated to be $10^{11} – 10^{12}$ m^{-2}, and the maximum value is about $5.2x10^{12}$ m^{-2}.

Let us examine the distribution of the characteristic angles of dislocations on the B4 slip system. In the present analysis, dislocation densities are evaluated in each finite element. If we multiply dislocation density by volume of an element, the product will give the length of dislocation segment in that element. Summation of such segment lengths over all elements will give the total length of dislocation segments in the entire specimen. Fig. 6 shows the total segment length of dislocations on the B4 slip system plotted against the characteristic angle of the segment. There are four distinct peaks of P1, P2, P3 and P4 at $+/- \pi/3$ and $+/- 2\pi/3$ and also two peaks of moderate magnitude at 0 and π. Peak P3, for example, shows that the total

length of dislocation segments, whose characteristic angles range form $\pi/3-\pi/18$ to $\pi/3+\pi/18$, is about 6.4 μm when the average volumetric strain is 0.199%. The essential features of the distribution do not change for 0.095% and 0.199% strain, indicating that the dislocation structure simply grows with deformation without change in its basic shape and arrangement. Groups of dislocation segments with characteristic angles +/- $\pi/3$ (peaks P2 and P3) contribute to the formation of one pair of groups on one side of the micro void, as shown in Fig. 5, and segments with angles +/- $2\pi/3$ contribute to the formation of the other pair of groups on the opposite side of the void.

Fig. 7 schematically shows the arrangements of two groups of dislocation segments on one side of the void. Extra-half planes of the dislocations in one group, which make peak P3 in Fig. 6, are opposed to those of the dislocations in the other group, making peak P2. On the opposite side of the void, dislocation segments with characteristic angles - $2\pi/3$ and $2\pi/3$ make two groups, and their extra-half planes, again, exist between the two groups.

Fig. 8 shows the GN dislocations obtained for the slip systems B4 and D4 when the average volumetric strain is 0.199%. Slip systems B4 and D4 have the same slip directions but different slip planes. Therefore, D4 slip system is the cross slip system of the B4 slip system, and vice versa. The inset in Fig. 8 schematically shows the viewpoint of Fig. 8 and the arrangement of slip planes of the two slip systems. Dislocation segments form a rhombus-shaped loop structure. Fig. 9 schematically shows the structure: each edge of the rhombus-shaped loop consists of a group of dislocation segments with similar characteristic angles, and one pair of opposing edges of

the rhombus belongs to the B4 slip system and the other pair belongs to the D4 system. Characteristic angles of most dislocation segments within four edges of the rhombus are close to +/- $\pi/3$ for the B4 system and +/- $2\pi/3$ for the D4 system. Extra-half planes of the dislocation segments on the four edges all exist inside the loop, indicating that this loop surrounds a platelet of a stacking fault of the interstitial type. The loop structure does not lie on one plane, but its shape is a creased rhombus.

The crystallographic process of the formation of prismatic dislocation loops is usually understood as generation of dislocation half loops on a slip system due to localized slip and annihilation of the screw segment of the loop after cross slip (Ashby and Johnson, 1969). In the molecular dynamics simulation by Rudd and Belak (2002a), the process was rather complex but prismatic loops sometimes seemed to be formed due to simultaneous activation of more than one slip system. Theoretically, simultaneous activation of one slip system and its cross slip system can lead to the formation of prismatic dislocation loops without the process of cross slip of screw segments on one system to the cross slip system. The present analysis does not account for the process of cross slip, but the resultant structure of dislocations shows close similarity to the prismatic dislocation loops observed in experiments or atomistic simulation.

4.2 Rough estimate of material transport by prismatic dislocation loops

Let us estimate the order of the number of atoms that are removed from the surface of the micro void and move with the prismatic dislocation loops. If we assume that a single prismatic loop is formed on one side of the micro

void, the length of the edge of the rhombus-shaped loop will be close to the total length of the dislocation segments with characteristic angle +/- $\pi/3$ or +/- $2\pi/3$, which is about 6.4 μm when the average volumetric strain is 0.199% (Fig. 6). This length divided by the lattice constant, for which we use a typical value of 0.3 nm, will be on the order of 10^4. The number of atoms surrounded by the prismatic dislocation loop will therefore be on the order of 10^8.

Two prismatic dislocation loops are formed in front and at the back of the void by the combination of slip deformation on the B4 and D4 systems. Similar to this, five combinations of slip deformations on slip systems A2-B2, A6-D6, A3-C3, D1-C1 and B5-C5 also develop similar structures of dislocations. Therefore, twelve loops of rhombus-shaped dislocation structures are formed around the void. These structures are all prismatic dislocation loops that bear extra-half planes inside the loop and contribute to material transport during the process of deformation. The total number of atoms moved by all of the prismatic dislocation loops will therefore be on the order of 10^9. In the next section, we will see that the total segment length of dislocations increase almost linearly with increase in average volumetric strain. This means that atomic transport increases in a parabolic manner with increase in average volumetric strain.

Let us discuss the relation between the size of the void and the number of atoms transported by the prismatic dislocation loops. If the representative length of the void changes from D to D' ($=D\times N$), that is, the void size is N-times larger than the one shown in Fig. 4, the density ρ' of the GN dislocations will be $1/N$-times smaller than that obtained in the present analysis, because the density is calculated by the spatial gradient of plastic shear strain.

At the same time, the element volume v_e' will be $v_e \times N^3$. The total dislocation segment length l' on the B4 slip system with the characteristic angle $\varphi=\pi/3$, for example, is calculated as

$$l' = \sum \rho' \cdot v_e' = \sum (\rho / N) \cdot (v_e \cdot N^3) = N^2 \sum \rho \cdot v_e = N^2 l \,. \qquad (14)$$

Since the number of atoms emitted from the void is proportional to l'^2, it scales with N^4.

4.3 Dislocation structure in a strain—hardening crystal

Next, we examine the dislocation structure in model II, in which slip systems harden by plastic slip. Fig. 10 shows the evolution of negative hydrostatic pressure plotted against average volumetric strain. The negative hydrostatic pressure in the model I saturates at about 33 MPa when the average volumetric strain is larger than 0.1%, while it increases monotonically in model II even after deformation of 1% volumetric strain. The density of GN dislocations on the B4 slip system at deformation stages A and B, shown in Fig. 10, with average volumetric strains of 0.63 and 1.72%, respectively, ranges from 10^{10} – 10^{13} m^{-2}, and the maximum values for deformation stages A and B are 3.5×10^{13} and 1.0×10^{14} m^{-2}, respectively. Fig. 11(a) shows the distribution of the total length of dislocation segments on the slip system B4. When the average volumetric strain is 0.63%, the distribution appears to be formed from peaks centered at +/- $\pi/2$, +/- $\pi/3$, +/- $2\pi/3$, 0 and π. When the average volumetric strain is 1.72%, peaks at +/- $\pi/2$ are dominant and there are

sub-peaks at +/- 2π/9, and +/- 7π/9. Fig. 11(b) shows the distribution of the total segment length on slip system A6. The essential features of the distribution and its growth with deformation are similar to those for slip system B4, although the distribution in the case of slip system A6 is more complex. Fig. 12 shows the development of the total length of dislocation segments with characteristic angles φ=π/2 and π/3. On the B4 slip system, the growth of dislocation segments with φ=π/2 is faster than that with φ=π/3, indicating that rhombus-shaped prismatic dislocation loops are made mainly from pure edge dislocations. It is easily understood that prismatic dislocation loops made from pure edge-type dislocations are *not* creased, unlike those described in section 4.1 and illustrated in Fig. 9. The peaks at φ=+/- π/2 (Fig. 11(a)) are not sharp enough at this deformation stage, and this makes it difficult to draw a simple picture for the structure of prismatic dislocation loops. One possible reason for this complex structure of dislocations is that emission of dislocations with various characteristic angles is essential for material with strain hardening and at a deformation stage of less than 2% of average volumetric strain. Actually, dislocations on the B4 slip system with characteristic angle φ= π/2 grow faster than those with other characteristic angles, and the population of dislocation segments on the A6 system with characteristic angle φ= π/2 exceeds that of dislocation segments with other characteristic angles at volumetric strain of about 1.6%. Another possible reason is that the spatial resolution of the present numerical analysis is not sufficient, and some numerical errors arise. We are not able to check and discuss further the latter possibility at present because the computing time needed for analysis with finer mesh is quite large. These points should be studied further.

5. Summary

Slip deformation in FCC metal single crystals with spherical-shaped micro voids was analyzed by a crystal plasticity technique, and growth of the geometrically necessary dislocations was examined. The results obtained are summarized as follows:

(1) GN dislocations on a slip system and ones on its cross slip system formed rhombus-shaped dislocation loops. These loops were prismatic dislocation loops of interstitial type, and they contributed to material transport from the micro void. The number of atoms moved by the prismatic dislocation loops, which formed around a micro void of 4 μm in diameter, was estimated to be on the order of 10^9 when the average volumetric strain was about 0.2%. The number of atoms moved with the formation of prismatic dislocation loops was estimated to increase in a biquadratic manner with increase in the size of the micro void.

(2) The total length of dislocation segments that were emitted with the slip process at a micro void increased monotonically with increase in average volumetric strain. The total length of dislocation segments plotted against characteristic angles of the segments in a material model with no-strain-hardening character showed significant peaks at +/- $\pi/3$ and +/- $2\pi/3$ mixed-type dislocation segments. When the material had a strain-hardening character, dislocation segments with a variety of characteristic angles were emitted at an early stage of deformation, and the population of pure edge-type dislocations grew faster with the progress of deformation.

REFERENCES

Ashby, M.F. and Johnson, L., 1969, Phil. Mag., 20, 1009.

Baaser, H., Gross, D., 2003. Analysis of void growth in a ductile material in front of a crack tip, Comp. Mat. Sci., 26, 28-35.

Belak, J., 1998a. Molecular dynamics simulation of high strain-rate void nucleation and growth in copper, CP429, Shock compression of condensed matter – 1997, Eds. Schmidt, Dandekar and Forbes, The American Inst. Phys., 211-214.

Belak, J., 1998b. On the nucleation and growth of voids at high strain-rates, J. Comp. Aided Mat. Design, 5, 193-206.

Belak J., Minich, R. 1999. Simulation of void growth at high strain-rate, Mat. Res. Soc. Symp. Proc. 539, 257-261.

Bonfoh, N., Lipinski, P., Carmasol, A., Tiem, S., 2004. Micromechanical modeling of ductile damage of polycrystalline materials with heterogeneous particles, Int. J. Plasticity, 20, 85-106.

Hill, R., 1966. Generalized constitutive relations for incremental deformation. J. Mech. Phys. Sol. 14, 95-102.

Kuhlmann-Wilsdorf, D., 1989. Theory of plastic deformation: properties of low energy dislocation structures, Mat. Sci. Eng., A113, 1.

Li, Z., Guo, W., 2002. The influence of plasticity mismatch on the growth and coalescence of spheroidal voids on the bimaterial interface, Int. J. Plasticity, 18, 249-279.

Li, Z., Wang, C., Guo, W., 2003. The evolution of voids in the plasticity strain hardening gradient materials. Int. J. Plasticity 19, 213-234.

Lubarda, V.A., Schneider, M.S., Kalantar, D.H., Remington, B.A., Meyers, M.A., 2004. Void growth by dislocation emission, Acta Mat., in press.

Moriarty, J.A., Belak, J, Rudd, R.E., Soederlind, P., Streitz, F.H., Yang, L.H., 2002. Quantum-based atomistic simulation of materials properties in transition metals, J. Phys.: Condens. Matter 14, 2825-2857.

Ohashi, T., 1987. Computer simulation of non-uniform multiple slip in face centered cubic bicrystals. Trans. Japan Inst. Metals. 28, 906-915.

Ohashi, T., 1994. Numerical modeling of plastic multislip in metal crystals of f.c.c. type. Phil. Mag. A70, 793-803.

Ohashi, T., 1997. Finite-element analysis of plastic slip and evolution of geometrically necessary dislocations in fcc crystals. Phil. Mag. Lett. 75, 51-57.

Ohashi, T., 1999. Evaluation and visualization of geometrically necessary dislocations in metal microstructures by means of continuum mechanics analysis. J. Phys. IV France. 9, Pr9-279-284.

Ohashi, T., Asakawa, K., 2002. Three dimensional dislocation structure formed in the vicinity of spherical inclusions. Trans. Japan Society for Mechanical Engineers. 68, 1513-1519 . (written in Japanese)

Ohashi, T., 2002. Formation of prismatic dislocation loops by dilatation of precipitates, Proc. 14th USNCTAM, Blacksburg, p342.

Ohashi, T., 2004a. Three dimensional structures of the geometrically necessary dislocations in matrix-inclusion systems under uniaxial tensile loading, Int. J. Plasticity, 20, 1093-1109.

Ohashi, T., 2004b. Solid mechanics and its applications, vol. 115, A new model of scale dependent crystal plasticity analysis, Proc. IUTAM symposium

on mesoscopic dynamics in fracture process and strength of materials, Osaka, Japan, Kluwer Academic Pub., Dordrecht, eds., H. Kitagawa and Y. Shibutani, 97-106.

Orsini, V.C., Zikry, M.A., 2001. Void growth and interaction in crystalline materials, Int. J. Plasticity, 17, 1393-1417.

Rudd, R.E., Belak, J., 2002. Multiscale modeling of plastic deformation in void growth and fracture, Proc. 14th USNCTAM, Blacksburg,, p347.

Rudd, R.E., 2002. Void nucleation and associated plasticity in dynamic fracture of polycrystalline copper: an atomistic simulation, Comp. Mat. Sci., 24, 148-153.

Schacht, T., Untermann, N., Steck, E., 2003. The influence of crystallographic orientation on the deformation behaviour of single crystals containing microvoids, Int. J. Plasticity, 19, 1605-1626.

Simmons, G., Wang, H., 1971. Single crystal elastic constants and calculated aggregate properties, 2nd ed., MIT press, Cambridge, 23.

Siruguet, K., Leblond, J-B., 2004. Effect of void locking by inclusions upon the plastic behavior of porous ductile solids – I: theoretical modeling and numerical study of void growth, Int. J. Plasticity, 20, 225-254.

Tvergaard, V., Niordson, C., 2004. Nonlocal plasticity effects on interaction of different size voids, Int. J. Plasticity, 20, 107-120.

Weertman, J., 2002. Anomalous work hardening, non-redundant screw dislocations in a circular bar deformed in torsion, and non-redundant edge dislocations in a bent foil, Acta Mat., 50, 673-689.

Yamada, Y., Yoshimura, N., Sakurai, T., 1968. Plastic stress-strain matrix and its application for the solution of elastic-plastic problems by the finite

element method, Int. J. Mech. Sci., 10, 343-354.

Zienkiewicz, O.C., 1977. The finite element method, third edition, McGraw-Hill, London, p141.

Postal address of the author

Tetsuya OHASHI,

Mechanical Systems Department, Kitami Institute of Technology,

Koencho 165, Kitami, Hokkaido 090-8507, Japan

Figure captions

Fig. 1. The tangent vector **l** and the characteristic angle φ of dislocation segments.

Fig. 2. A dislocation loop made up from dislocation segments. Each dislocation segment is shown by a color, determined as a function of the characteristic angle.

Fig. 3. Definitions of the length and thickness of dislocation line segments used in the graphical representation of a dislocation structure. $\overline{v}$ is a constant and 3.375 μm^3 is used in the present paper.

Fig. 4. Geometry of the model employed in this paper. A void region is centered in the matrix region, and its volume fraction is about 0.12%.

Fig. 5. Geometrically necessary dislocations on the B4 slip system observed in model I when the average volumetric strain is about 0.053% (a), and 0.199% (b) and (c). In this graphical representation, values for d_1, d_2 and d_3 are 1×10^{10}, 1×10^{12} and 8×10^{12} m^{-2}, respectively.

Fig. 6. Histogram of the characteristic angles φ of dislocation segments on the B4 slip system observed in model I when the average volumetric strains are about 0.095% (gray-colored bars) and 0.199% (black-colored bars).

Fig. 7. Schematic illustration of groups of dislocation segments on the B4 slip system observed on one side of the micro void in model I specimen. Extra-half planes of the dislocation segments exist between the groups of the dislocation segments.

Fig. 8. Geometrically necessary dislocations on the B4 and the D4 slip

systems observed in model I when the average volumetric strain is about 0.199%. Values for d_1, d_2 and d_3 are 1×10^{10}, 1×10^{12} and 8×10^{12} m^{-2}, respectively. Slip systems B4 and D4 are cross slip systems to each other (Slip planes of the B4 and D4 systems are not the same, but they have the same slip directions.).

Fig. 9. Schematic illustration of rhombus-shaped prismatic dislocation loops shown in Fig. 8. Dislocation segments on the B4 slip system with φ =+/- π/3 and those on the D4 system with φ =+/- 2π/3 make up the structure. Extra-half planes of the dislocation segments are surrounded by these dislocation segments.

Fig. 10. Change in negative hydrostatic pressure in models I and II.

Fig. 11. Total length of the dislocation segments on slip systems B4 (a) and A6 (b) in model II when the average volumetric strains are 0.63% and 1.72%.

Fig. 12. Evolution of the total length of dislocations with characteristic angles φ = π/3 and π/2. The evolution is approximately linear within the range analyzed in this study. On slip system B4, pure edge dislocations develop faster than those with other characteristic angles, while on slip system A6, the dislocation structure is complex, consisting of dislocation segments with various characteristic angles.

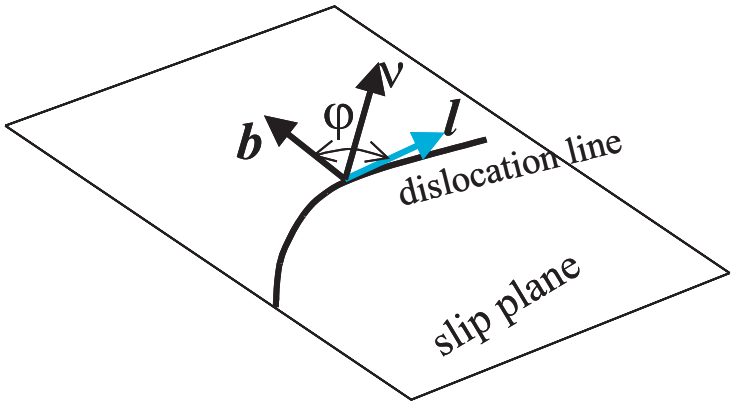

Fig. 1

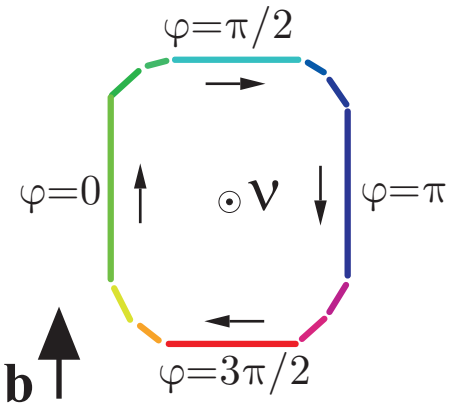

Fig. 2

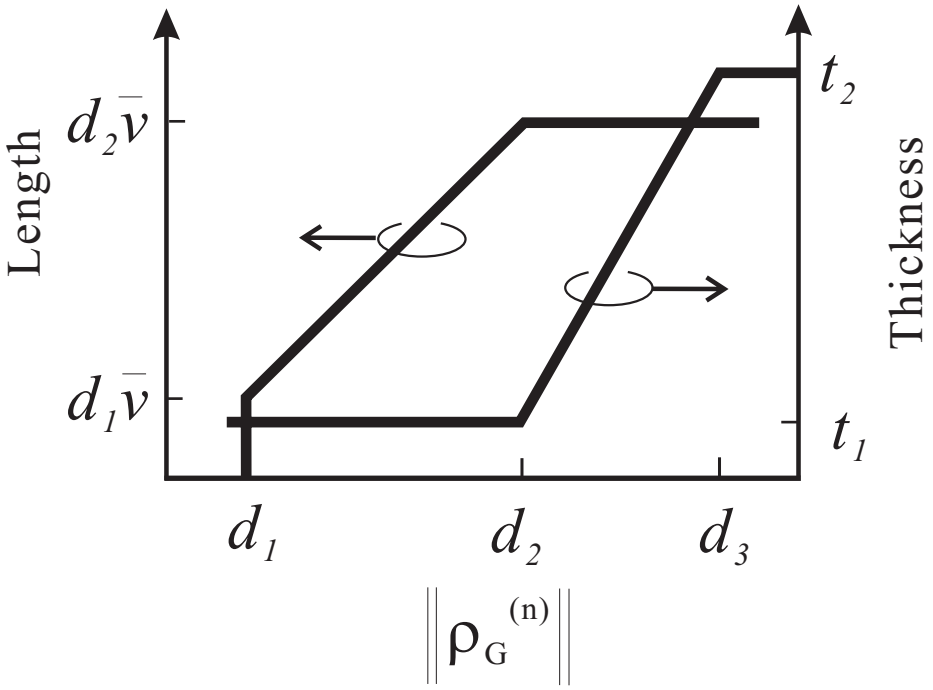

Fig. 3

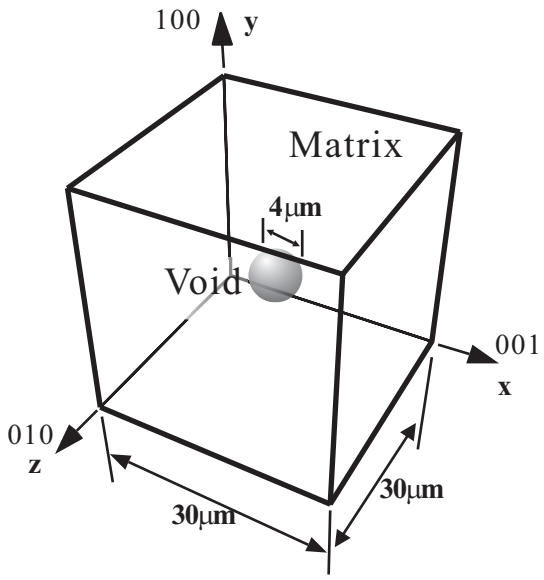

Fig. 4

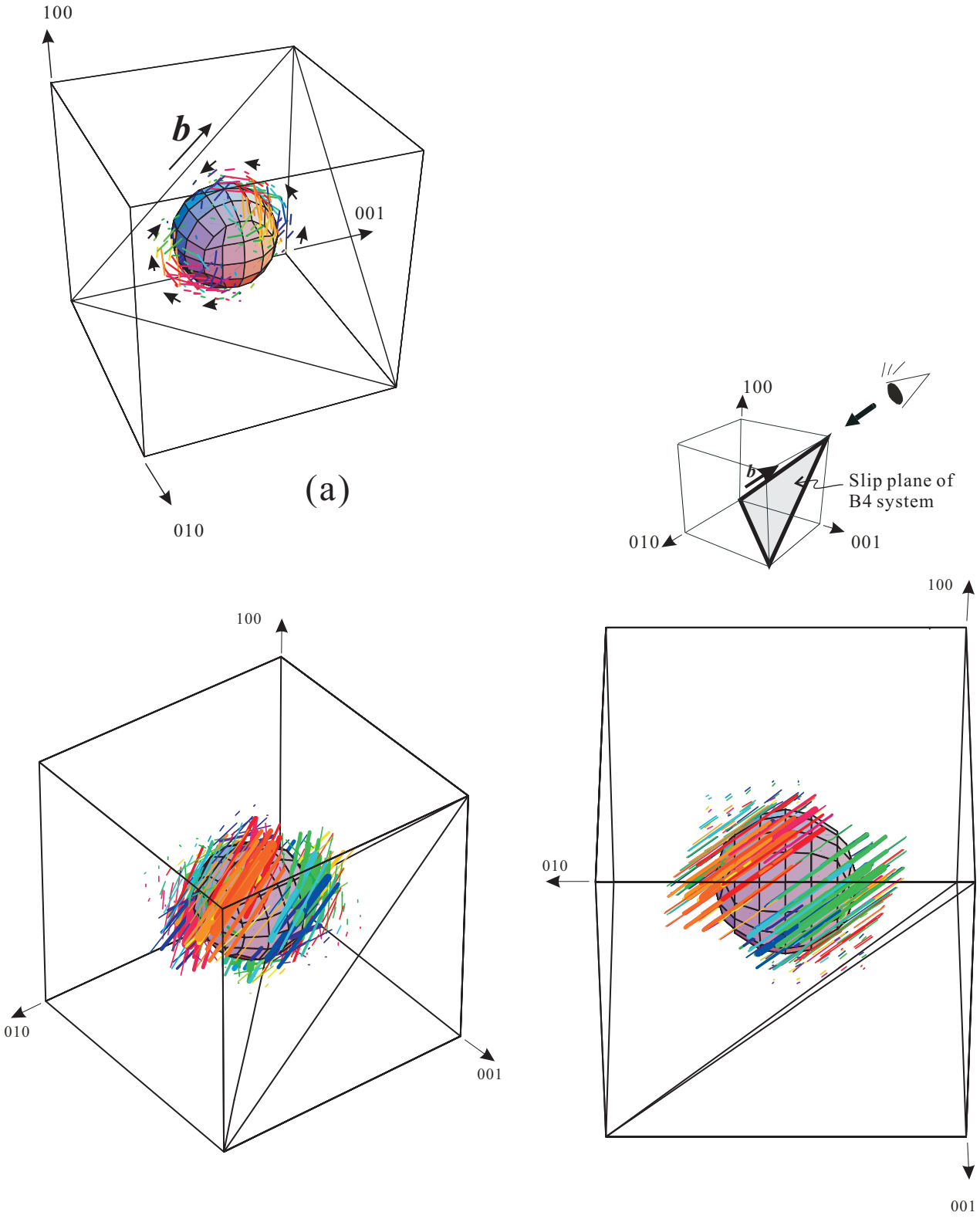
100
b
001
010
(a)
100
b
Slip plane of
B4 system
010
001
100
010
001
(b)
100
010
001
(c)

Fig. 5

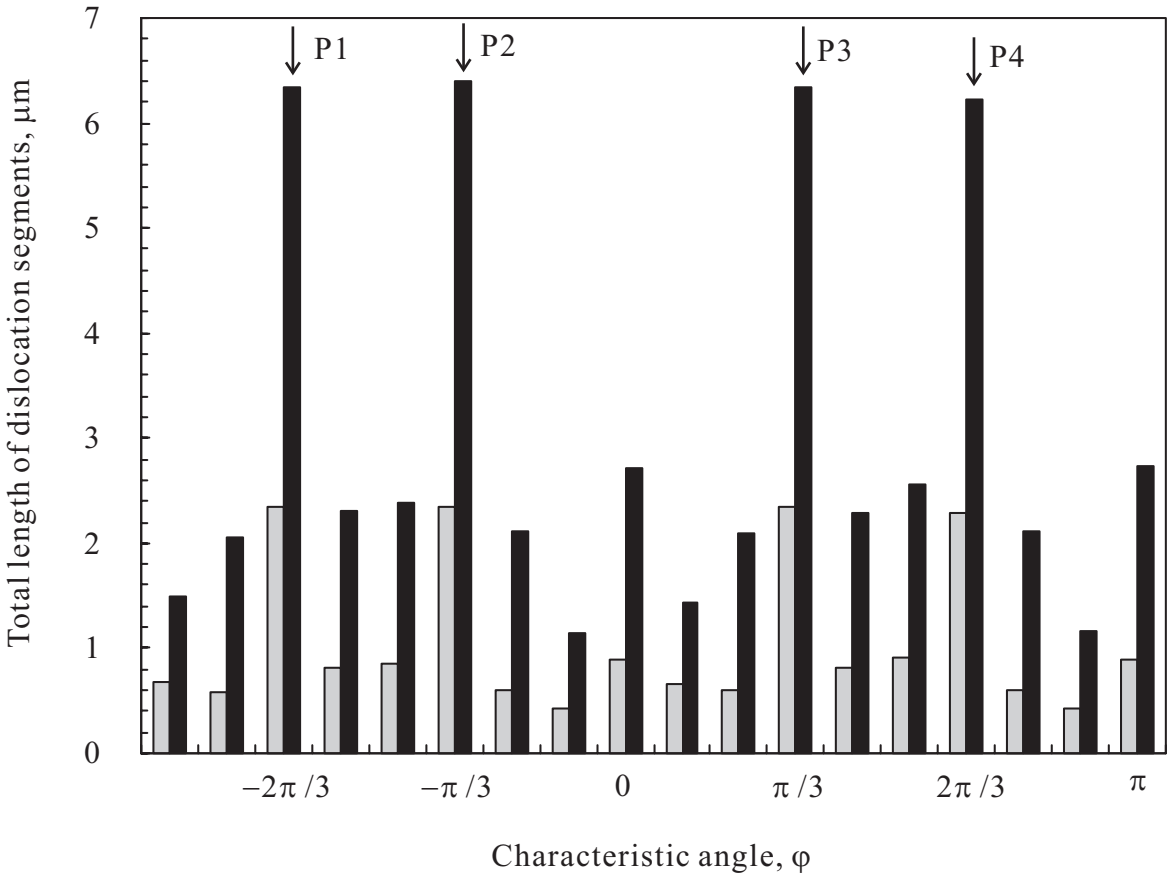
Total length of dislocation segments, μm
7
6
5
4
3
2
1
0
P1
P2
P3
P4
−2π /3
−π /3
0
π /3
2π /3
π
Characteristic angle, φ

Fig. 6

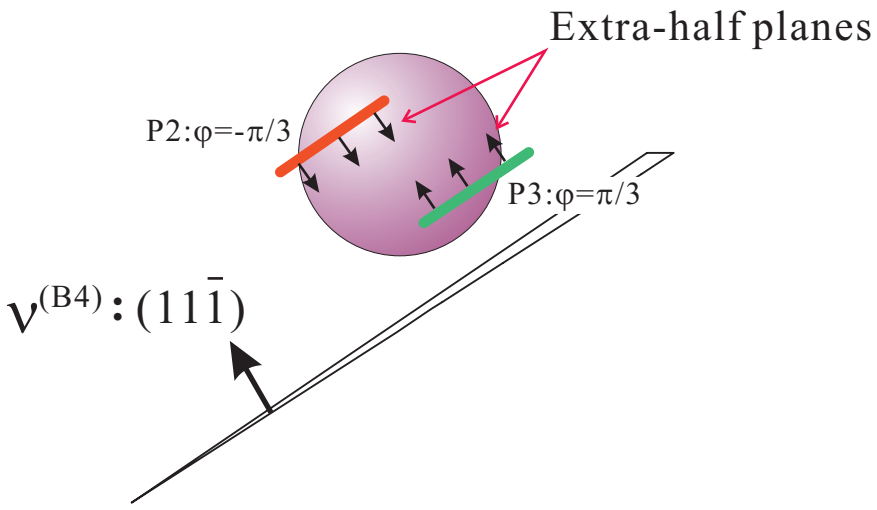

Fig. 7

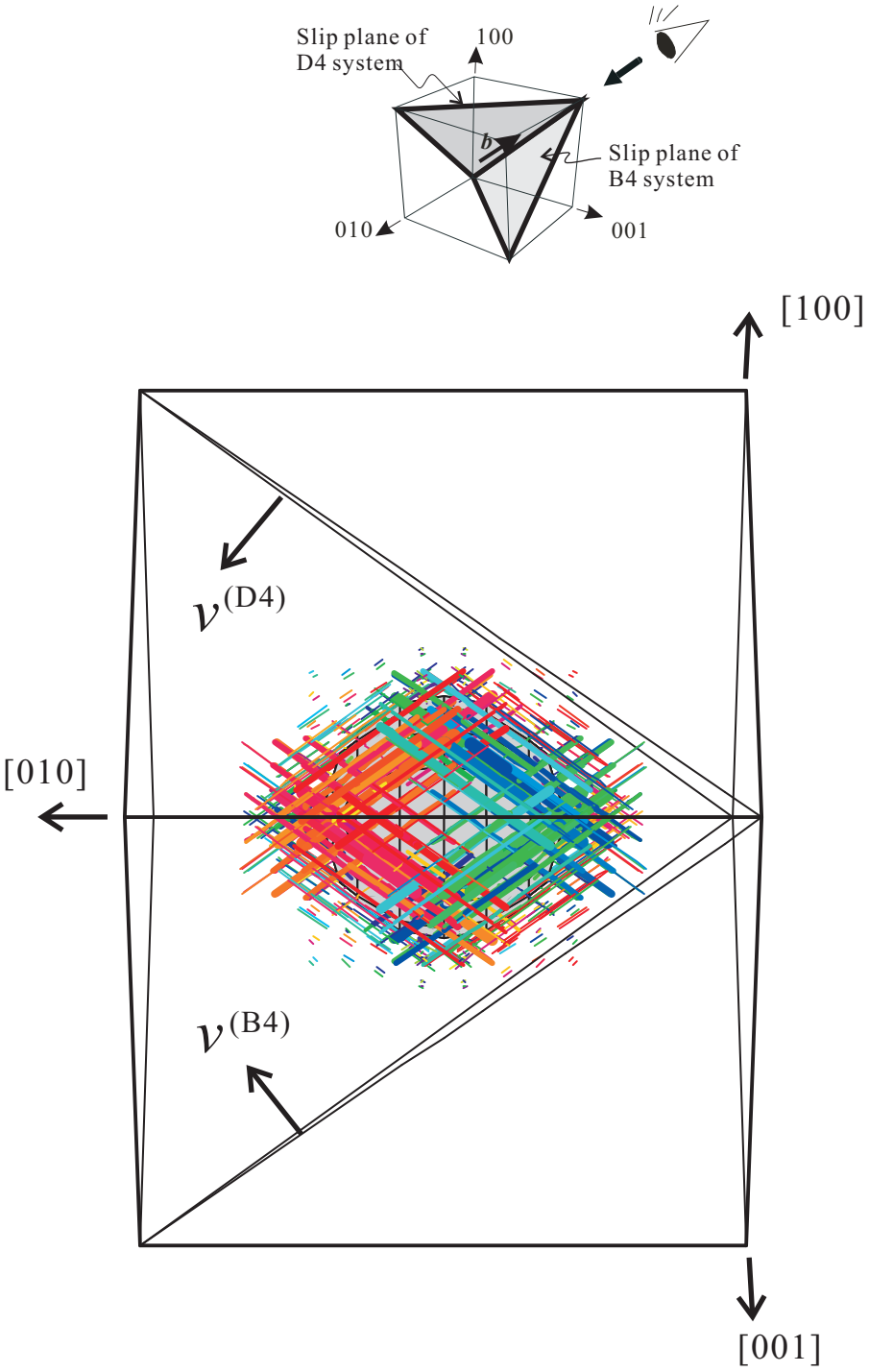
Slip plane of
D4 system
100
b
Slip plane of
B4 system
010
001
[100]
$v^{(D4)}$
[010]
$v^{(B4)}$
[001]

Fig. 8

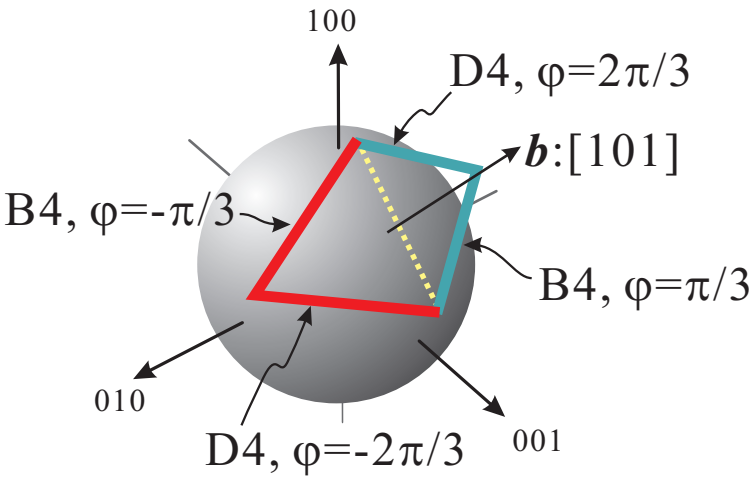

Fig. 9

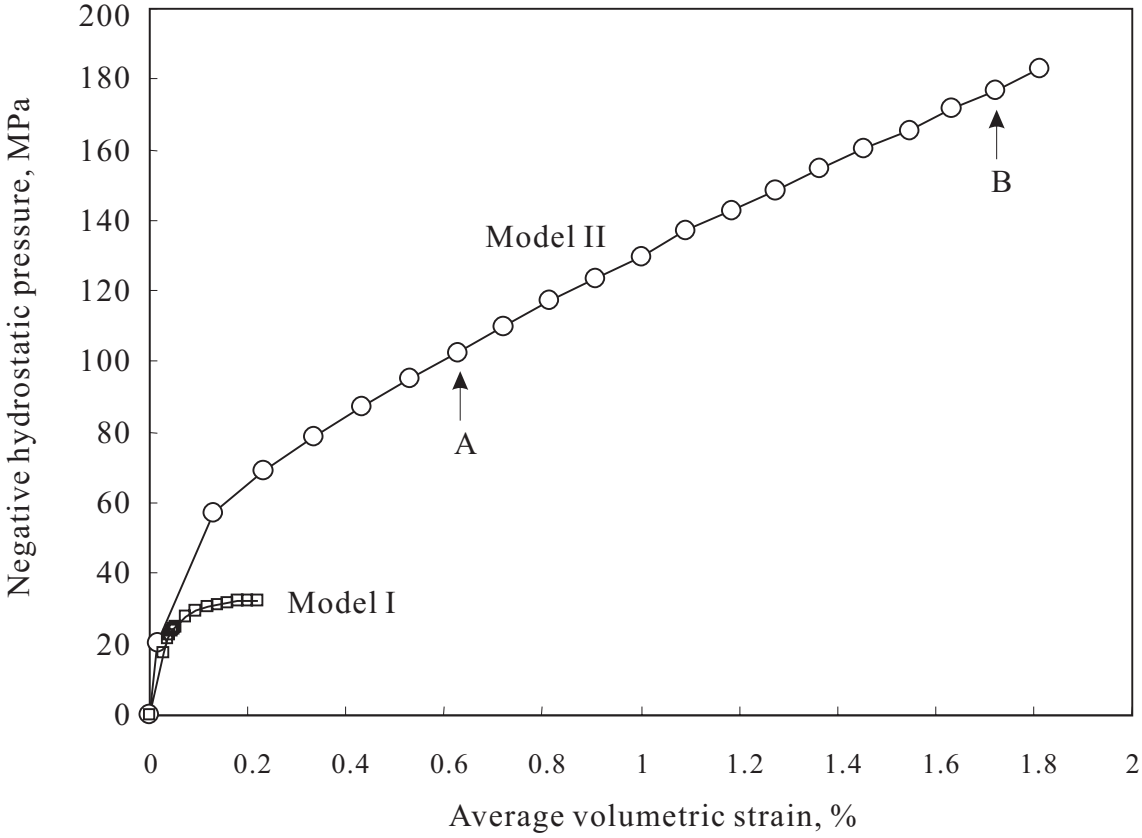
Negative hydrostatic pressure, MPa
200
180
160
140
120
100
80
60
40
20
0
0
0.2
0.4
0.6
0.8
1
1.2
1.4
1.6
1.8
2
Average volumetric strain, %
Model II
Model I
A
B

Fig. 10

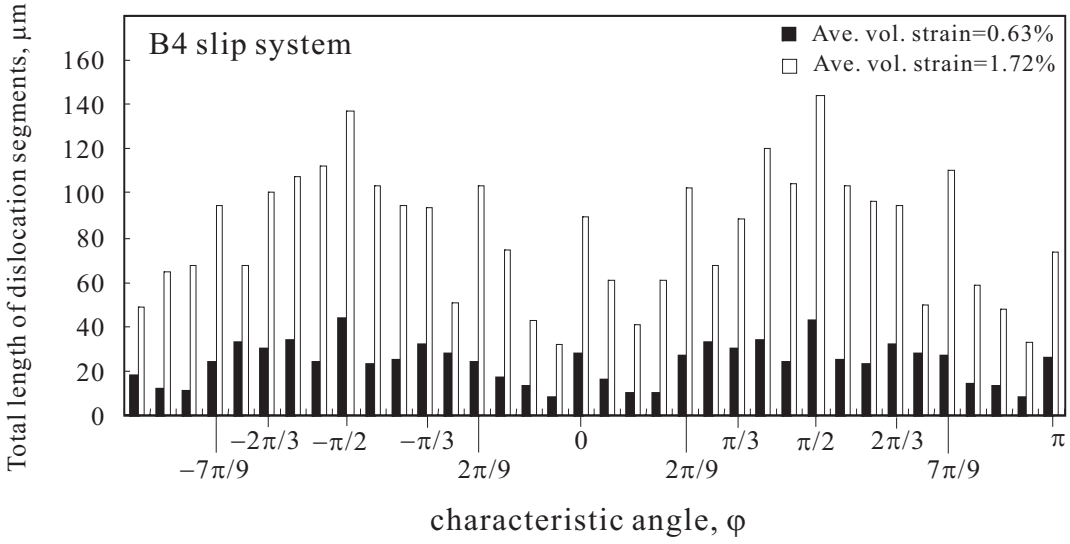
B4 slip system
Ave. vol. strain=0.63%
Ave. vol. strain=1.72%
Total length of dislocation segments, μm
0
20
40
60
80
100
120
140
160
−7π/9
−2π/3
−π/2
−π/3
2π/9
0
2π/9
π/3
π/2
2π/3
7π/9
π
characteristic angle, φ

(a)

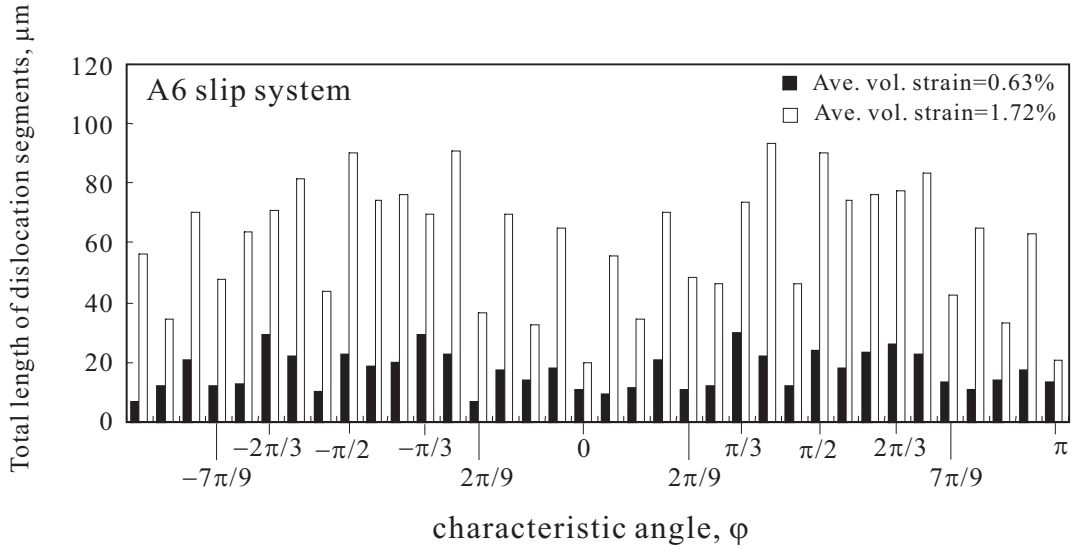
A6 slip system
Ave. vol. strain=0.63%
Ave. vol. strain=1.72%
Total length of dislocation segments, μm
0
20
40
60
80
100
120
−7π/9
−2π/3
−π/2
−π/3
2π/9
0
2π/9
π/3
π/2
2π/3
7π/9
π
characteristic angle, φ

(b)

Fig. 11

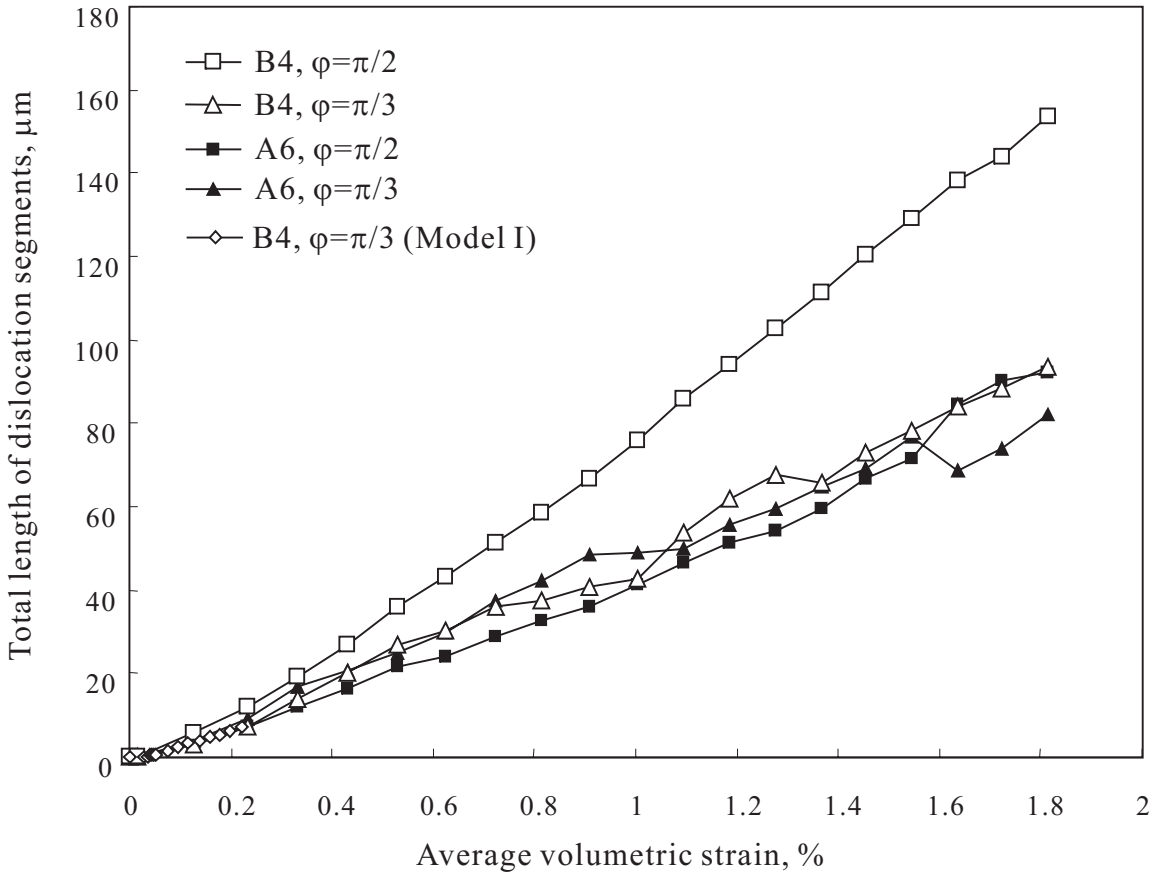
Total length of dislocation segments, μm
Average volumetric strain, %
B4, φ=π/2
B4, φ=π/3
A6, φ=π/2
A6, φ=π/3
B4, φ=π/3 (Model I)
0
20
40
60
80
100
120
140
160
180
0
0.2
0.4
0.6
0.8
1
1.2
1.4
1.6
1.8
2

Fig. 12